Congreso de Métodos Numéricos en Ingeniería 2009
Barcelona, 29 junio al 2 de julio 2009

3D BEHAVIOUR OF A 4 PARAMETER ISOTROPIC NONLINEAR HARDENING PLASTICITY MODEL FOR CONCRETE

Eduardo B. Pereira[1*], Joaquim A. O. Barros[2]

1: ISISE,Department of Civil Engineering
School of Engineering
University of Minho
4800-058 Guimarães - Portugal
e-mail: eduardo.pereira@civil.uminho.pt, web: http://www.civil.uminho.pt/composites
2: ISISE,Department of Civil Engineering
School of Engineering
University of Minho
4800-058 Guimarães - Portugal
e-mail: barros@civil.uminho.pt web: http://www.civil.uminho.pt/composites

Keywords: Elastoplasticity, concrete, finite element method

Abstract. *In general, concrete is a highly nonlinear material with great dependence on the confining stresses, a type of behaviour also common in other granular and quasi-brittle materials. The CEB-FIP Model Code [1] recommends the use of a four-parameter failure criterion to estimate the strength of concrete under multiaxial states of stress. This failure criterion is also known as the Ottosen failure criterion, and it captures with high accuracy the behaviour of these materials, as demonstrated by several researchers, performing experimental test programs. The concrete strength estimation takes into account, with great precision, the effect of the increase in the confining stresses. In order to simulate the monotonic quasi-static multiaxial behaviour of concrete, one possible strategy is to introduce in this failure criterion a hardening parameter and the corresponding evolution law, under the isotropic behaviour framework. In the present work, the concrete compressive strength in the Ottosen failure criterion is assumed as the hardening parameter, and the CEB-FIP Model Code 90 law for the uniaxial nonlinear behaviour of concrete is used to derive the hardening law. In this case, the loading surface is not explicitly defined as a function of the hardening parameter, as in the other more common and simpler isotropic models. As a consequence, some difficulties may emerge, mainly of a numerical nature. In this context, the formulation of the model in a thermodynamically consistent framework is presented. The general behaviour of this model is accessed by the simulation of the monotonic multiaxial loading of concrete elements, and its numerical efficiency is discussed.*

1 INTRODUCTION

When analysing the behaviour of concrete structures, it is important to identify failure of concrete due to the occurrence of certain combinations of the stress components in a certain part of the structure. The interaction of the various components of the state of stress in concrete determines its strength. Simple tensile, compressive or shear stresses can not be used separately as failure criteria, since the limiting values of each of these material properties will depend on all stress components. Consequently, the concept of an interaction mathematical equation that allows the separation of the stress space into the admissible and the non-admissible states is very comfortable. Thanks to the pioneering works of Tresca, von Mises and several others, plasticity developed some decades ago as a scientific field in solid mechanics. Several interaction functions, called failure criteria, have been proposed for different materials including concrete, assuming the shape of surfaces in the 3D stress space. The very well known highly non-linear behaviour of concrete keeps being a great challenge for material and structural disciplines trying to predict and simulate it. Formulations based on fracture mechanics, damage or plasticity have been proposed for decades, and their complexity gradually increased with time. The perfect model is though, even theoretically, unreachable, given the complexity of mechanical behaviour and strength of disordered materials, like concrete. If such a kind of model would exist, its huge complexity would compromise its efficiency. A good balance between performance and accuracy has always to be found.

1.1 Failure criteria for Concrete

Since the previous works of Kupfer it is recognized that the experimental results of concrete tested under multiaxial loading are best fit by the failure surfaces depending on all three stress invariants (I1, J2 and J3) [2]. The hydrostatic pressure dependence and the interaction between shear and tangential stresses in concrete are properly taken into account in this fashion. The first models applied to concrete were very simple and approximated, because they were only taking into account the influence of hydrostatic pressure. The Rankine criterion, in the class of the one-parameter models (with the maximum tensile stress determining failure), or the Mohr-Coloumb criterion, in the class of two-parameter models (with failure determined by both cohesion and the internal friction angle), had straight-line envelopes in the meridian planes and non-smooth 3D surfaces. Some later three-parameter models were able to propose smooth solutions for the failure surface, like the William-Warnke criterion, but they were still preserving the straight-lines envelope in the meridian planes.

The four-parameter model proposed by Ottosen in 1975 [3], while depending on the three stress invariants (I1, J2 and J3), showed good ability to fit the experimental biaxial results of Kupfer *et al* [4]. Smoothness, convexity, curved meridians and a gradual transition from an almost triangular shape to almost circular in the deviatoric plane with the increase of hydrostatic pressure make the Ottosen failure criterion very appropriate for the simulation

of concrete failure (see fig. 1). Adding to this is the fact that, at the moment, the Ottosen yield criterion is the one recommended by [1] to determine the failure of concrete under any 3D stress components combination. This criterion is represented by the following equation:

$$f(\boldsymbol{\sigma}, \tilde{\sigma}) = \left[\alpha J_2 + \sigma_c \left(\lambda\sqrt{J_2} + \beta I_1\right)\right]^{\frac{1}{2}} - \sigma_c \tag{1}$$

Furthermore, the identification of the model parameters from standard tests is relatively simple. For all these reasons, the Ottosen failure surface is usually one of the preferred criteria to assess the multiaxial behaviour of concrete, disregarding some of the new and more sophisticated models proposed for particuar situations by several reserchers ([5], [6], among others).

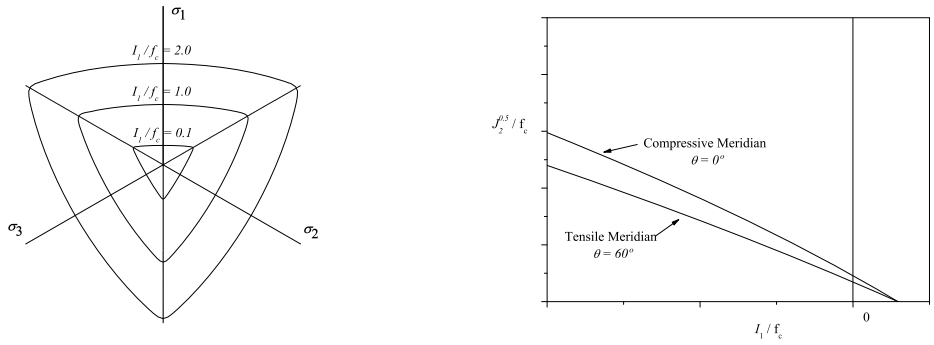

(a) (b)

Figure 1: Representation of the Ottosen yield criterion in the (a) deviatoric and (b) meridional (rendulic) planes, in the Haigh-Westergaard stress space.

1.2 Hardening

Perfect elastoplastic materials yield at a constant stress while subjected to uniaxial loading. During plastic flow under multiaxial loading, the stress state can move along the yield surface and the surface itself remains unchanged. The hardening/softening (referred as "hardening" in a broad sense) behaviour of concrete while in uniaxial loading is quite distant from this ideally (or perfect) elastoplastic type of behaviour. While plastic deformation is taking place, the stress level is not constant and it actually can increase (harden) or decrease (soften). Correspondingly, assuming that while plastic flow is taking place the stress state is moving along the yield surface, increasing/decreasing stress levels will determine changes in size and/or shape of the initial yield surface, the one that determined the beginning of the plastic process and usually designated as the elastic limit envelope. Intermediate states of the surface are then usually called loading surfaces.

The change of size/shape of the loading surface during hardening is usually characterized with the help of one or more parameters. Plastic flow with hardening generalizes the perfect plasticity in solids for which the yield or failure surface remains fixed in stress space. The hardening law defines, based on these parameters, the subsequent motion of the loading surfaces after yielding is reached. The simplest approach, (introduced by Odqvist [7]) known as isotropic hardening, determines the evolution of the loading surface in similar configurations with respect to the origin. It is, however, well known the weakness of this form of hardening to reproduce cyclic and reversed types of loading or directional anisotropy induced by plastic flow [8]. These are especially relevant in concrete, where kinematic and mixed hardening allow the better description of these particularities, with the associated cost of an increased number of parameters needed to characterize the expansion and translation of the loading surfaces.
In this work we are especially interested in assessing the utility and viability of the application of the Ottossen failure criterion as a loading surface. As such, we will restrict our study to the cases where monotonic static loading occurs. It is clear that an increased difficulty emerges when the Ottosen failure criterion is generalized in a hardening/softening framework, since the equation of the loading surfaces does not fits the general form of the isotropic models, where the hardening parameter is explicitly defined. For this reason, some particular measures are needed to formulate adequately the numerical implementation. Furthermore, there is a special interest in having a perspective on how a model based on the uniaxial compressive law and the multiaxial failure criterion, both proposed by [1], behaves.

2 NUMERICAL IMPLEMENTATION

The Ottosen yield criterion may be used as a loading surface when expressed as a function of the stress tensor $\boldsymbol{\sigma}$ and the hardening parameter $\tilde{\sigma}$, as described in the following [9]:

$$f(\boldsymbol{\sigma}, \tilde{\sigma}) = \left[\alpha J_2 + \tilde{\sigma}\left(\lambda\sqrt{J_2} + \beta I_1\right)\right]^{\frac{1}{2}} - \tilde{\sigma} \tag{2}$$

The stress tensor may be represented, in what is commonly called as the engineering form, by a six component vector in the (x, y, z) coordinate system.

$$\boldsymbol{\sigma} = \{\sigma_x \ \sigma_y \ \sigma_z \ \tau_{yz} \ \tau_{xz} \ \tau_{xy}\} \tag{3}$$

The hardening parameter is defined, in the present case, by a function based on the proposed law by [1] for uniaxial compression behaviour of concrete (see fig. 2). Considering the split of deformations in the elastic and the plastic part, this hardening law is obtained from the original [1] law by extracting the elastic deformation for each load level.
The Ottosen yield function parameters are mainly defined considering the uniaxial compressive and tensile strengths of the material. In the case of concrete, the [1] recommends

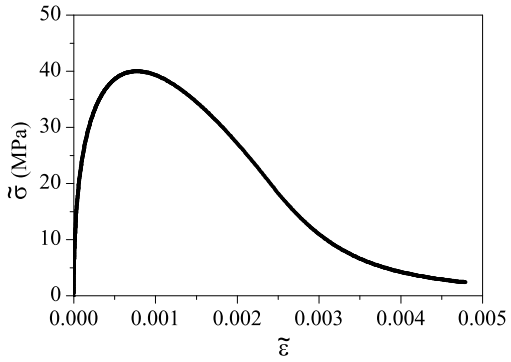

Figure 2: Hardening function for a concrete with $40MPa$ of compressive strength.

that uniaxial compressive and tensile strength medium values are used, that is, f_{cm} and f_{ctm} respectively. The referred parameters are described by the following equations:

$$\begin{aligned} \alpha &= \frac{1}{9K^{1.4}} \\ \beta &= \frac{1}{3.7K^{1.1}} \\ K &= \frac{f_{ctm}}{f_{cm}} \end{aligned} \tag{4}$$

and

$$\lambda = \begin{cases} c_1 \cos\left[\frac{\pi}{3} - \frac{1}{3}\arccos\left(-c_2 \cos 3\theta\right)\right] & \text{for} \quad \cos 3\theta \leq 0 \ , \\ c_1 \cos\left[\frac{1}{3}\arccos\left(c_2 \cos 3\theta\right)\right] & \text{for} \quad \cos 3\theta > 0 \ . \end{cases} \tag{5}$$

where,

$$\begin{aligned} c_1 &= \frac{1}{0.7K^{0.9}} \\ c_2 &= 1 - 6.8(K - 0.07)^2 \\ \cos 3\theta &= \frac{3\sqrt{3}}{2}\frac{J_3}{J_2^{\frac{3}{2}}} \end{aligned} \tag{6}$$

The I_1, J_2 and J_3 variables represent, respectively, the first, the second deviatoric and the third deviatoric stress invariants. The corresponding equations are, in the (x, y, z) coordinate system:

$$I_1 = \sigma_{xx} + \sigma_{yy} + \sigma_{zz}.$$

$$J_2 = \frac{1}{3}\left(\sigma_x^2 + \sigma_y^2 + \sigma_z^2 - \sigma_x\sigma_y - \sigma_x\sigma_z - \sigma_y\sigma_z + 3\tau_{yz}^2 + 3\tau_{xz}^2 + 3\tau_{xy}^2\right). \tag{7}$$

$$\begin{aligned} J_3 = \tfrac{2}{27}\left(\sigma_x^3 + \sigma_y^3 + \sigma_z^3\right) - \tfrac{1}{9}\left(\sigma_x^2\sigma_y + \sigma_x^2\sigma_z + \sigma_y^2\sigma_x + \sigma_y^2\sigma_z + \sigma_z^2\sigma_x + \sigma_z^2\sigma_y\right) \\ \tfrac{4}{9}\sigma_x\sigma_y\sigma_z - \tfrac{2}{3}\left(\sigma_x\tau_{yz}^2 + \sigma_y\tau_{xz}^2 + \sigma_z\tau_{xy}^2\right) + \tfrac{1}{3}(\sigma_x\tau_{xy}^2 + \sigma_x\tau_{xz}^2 + \\ \sigma_y\tau_{xy}^2 + \sigma_y\tau_{yz}^2 + \sigma_z\tau_{xz}^2 + \sigma_z\tau_{yz}^2) + 2\tau_{yz}\tau_{xz}\tau_{xy}\ . \end{aligned}$$

According to the plasticity theory principles, the flux vector $\boldsymbol{a}$ is composed by the six derivatives of the yield function with respect to each of the six stress components:

$$\boldsymbol{a} = \left\{ \frac{\partial f\left(\boldsymbol{\sigma}, \tilde{\sigma}\right)}{\partial \sigma_x} \quad \frac{\partial f\left(\boldsymbol{\sigma}, \tilde{\sigma}\right)}{\partial \sigma_y} \quad \frac{\partial f\left(\boldsymbol{\sigma}, \tilde{\sigma}\right)}{\partial \sigma_z} \quad \frac{\partial f\left(\boldsymbol{\sigma}, \tilde{\sigma}\right)}{\partial \tau_{yz}} \quad \frac{\partial f\left(\boldsymbol{\sigma}, \tilde{\sigma}\right)}{\partial \tau_{xz}} \quad \frac{\partial f\left(\boldsymbol{\sigma}, \tilde{\sigma}\right)}{\partial \tau_{xy}} \right\} \tag{8}$$

The equation that defines each of the six flux vector $\boldsymbol{a}$ components is, in indicial notation, the following:

$$a_i = \frac{\partial f\left(\boldsymbol{\sigma}, \tilde{\sigma}\right)}{\partial \sigma_i} = \frac{\alpha\dfrac{\partial J_2}{\partial \sigma_i} + \tilde{\sigma}\left(\dfrac{\partial \lambda}{\partial \sigma_i}\sqrt{J_2} + \dfrac{1}{2}\lambda\ J_2^{-\frac{1}{2}}\ \dfrac{\partial J_2}{\partial \sigma_i} + \beta\dfrac{\partial I_1}{\partial \sigma_i}\right)}{2\left[\alpha J_2 + \tilde{\sigma}\left(\lambda\sqrt{J_2} + \beta I_1\right)\right]^{\frac{1}{2}}} \tag{9}$$

For the entire definition of the flux vector $\boldsymbol{a}$, the first derivatives of the λ parameter with respect to the stress components must be defined. There is also the need to define the first derivatives of the stress invariants I_1 , J_2 and J_3 but, for the sake of clarity of this work, they will not be demonstrated since they can be easily derived.

2.1 The Return-mapping Algorithm

In the context of non-linear analysis by finte element method (FEM), the system of equilibrium equations is established in the incremental form. In this fashion, the stress increment for the new "load step" $n+1$, $\Delta\boldsymbol{\sigma}_{n+1}$, is defined by the constitutive relation established in the incremental form, where $\boldsymbol{D}$ represents the constitutive matrix, and $\Delta\boldsymbol{\epsilon}_{n+1}$ and $\Delta\boldsymbol{\epsilon}_{n+1}^p$ represent, respectivelly, the total strain and the plastic strain increments within the "load step" $n+1$:

$$\Delta\boldsymbol{\sigma}_{n+1} = \boldsymbol{D}\left(\Delta\boldsymbol{\epsilon}_{n+1} - \Delta\boldsymbol{\epsilon}_{n+1}^p\right) \tag{10}$$

At the onset of the new "load step", the total strain increment is known and comes from the main FEM iterative solving algorithm. The plastic strain increment, however, is yet unknown, and the procedure used in its determination within each "load step" will be discussed in the following sections. Following the ordinary framework of the implicit backward Euler algorithm, a first approximation to the solution, the trial stress increment is computed assuming the total strain increment as elastic, that is to say, the plastic strain increment is kept null and the total plastic strain at the "load step" $n+1$ is the same as the one of the former "load step", n. The hardening parameter is also assumed to preserve the value of the former load step:

$$\begin{aligned} \Delta\boldsymbol{\sigma}_{n+1}^{trial} &= \boldsymbol{D}\left(\Delta\boldsymbol{\epsilon}_{n+1} - \Delta\boldsymbol{\epsilon}_{n+1}^{p,\ trial}\right) \\ \boldsymbol{\sigma}_{n+1}^{trial} &= \boldsymbol{\sigma}_n + \Delta\boldsymbol{\sigma}_{n+1}^{trial} \\ \boldsymbol{\epsilon}_{n+1}^{p,\ trial} &= \boldsymbol{\epsilon}_n^p \\ \tilde{\sigma}_{n+1}^{trial} &= \tilde{\sigma}_n \end{aligned} \tag{11}$$

Following these assumptions, the initial value of the yielding function is computed for the trial values of "load step" $n+1$:

$$f_{n+1}^{trial} = f_{n+1}^{trial}\left(\boldsymbol{\sigma}_{n+1}^{trial}\ ,\ \ \tilde{\sigma}_{n+1}^{trial}\right) \tag{12}$$

Then, the two ranges of possible solutions determine the behaviour of the material. If the yield function assumes a non-negative value, and reminding that only static loading is being considered, then the material enters the elasto-plastic domain:

$$\begin{cases} \text{if} \ \ f_{n+1}^{trial} < 0 \quad \text{then} \quad \tilde{\sigma}_{n+1} = \tilde{\sigma}_{n+1}^{trial} \ \text{(elastic behaviour)} \ , \\ \text{if} \ \ f_{n+1}^{trial} \geq 0 \quad \text{then} \quad \tilde{\sigma}_{n+1} \neq \tilde{\sigma}_{n+1}^{trial} \ \text{(elasto-plastic behaviour)} \ . \end{cases} \tag{13}$$

Whenever the material enters the elasto-plastic domain, the total plastic strains and the internal variables have to change. In this fashion, their new values for the "load step" $n+1$ may be computed as follows:

$$\begin{cases} \boldsymbol{\epsilon}_{n+1}^p = \boldsymbol{\epsilon}_n^p + \Delta\boldsymbol{\epsilon}_{n+1}^p \quad \text{with} \quad \Delta\boldsymbol{\epsilon}_{n+1}^p = \Delta\lambda_{n+1}\ \dfrac{\partial f_{n+1}}{\partial\boldsymbol{\sigma}_{n+1}} \ , \\ \\ \tilde{\epsilon}_{n+1} = \tilde{\epsilon}_n + \Delta\tilde{\epsilon}_{n+1} \quad \text{with} \quad \Delta\tilde{\epsilon}_{n+1} = -\Delta\lambda_{n+1}\ \dfrac{\partial f_{n+1}}{\partial\tilde{\sigma}_{n+1}} \ . \end{cases} \tag{14}$$

In a thermodynamical framework, the second of eqs.(14), or the evolution law, is derived from the second thermodynamical law, or dissipation inequality, assuming the convexity

of the loading surface and that no thermal exchanges or viscous processes exist. For further details see [10].
Once the values of $\Delta\boldsymbol{\epsilon}^{p}_{n+1}$ are calculated, then the final state of stress $\Delta\sigma_{n+1}$ corresponding to load step $n+1$ may be computed, as follows:

$$\boldsymbol{\sigma}_{n+1} = \boldsymbol{\sigma}^{trial}_{n+1} - \boldsymbol{D}\Delta\boldsymbol{\epsilon}^{p}_{n+1} = \boldsymbol{\sigma}^{trial}_{n+1} - \Delta\lambda_{n+1}\ \boldsymbol{D}\frac{\partial f_{n+1}}{\partial\boldsymbol{\sigma}_{n+1}} \tag{15}$$

The use of the backward Euler integration scheme in a numerical framework implies the need to determine the $\Delta\boldsymbol{\epsilon}^{p}_{n+1}$ and $\Delta\tilde{\epsilon}_{n+1}$ by an iterative procedure. Within this procedure, the objective is to minimize the residues $r^{(k)}_{f,\ n+1}, r^{(k)}_{\boldsymbol{\epsilon},\ n+1}$ and $r^{(k)}_{\tilde{\epsilon},\ n+1}$, expressed by the following:

$$\begin{aligned}
r^{(k)}_{f,\ n+1} &= f^{(k)}_{n+1}\left(\boldsymbol{\sigma}^{(k)}_{n+1},\ \tilde{\sigma}^{(k)}_{n+1}\right)\\
r^{(k)}_{\boldsymbol{\epsilon},\ n+1} &= -\left(\boldsymbol{\epsilon}^{p}_{n+1}\right)^{(k)} + \boldsymbol{\epsilon}^{p}_{n} + \Delta\lambda^{(k)}_{n+1}\ \frac{\partial f^{(k)}_{n+1}}{\partial\boldsymbol{\sigma}^{(k)}_{n+1}}\\
r^{(k)}_{\tilde{\epsilon},\ n+1} &= -\left(\tilde{\epsilon}_{n+1}\right)^{(k)} + \tilde{\epsilon}_{n} - \Delta\lambda^{(k)}_{n+1}\ \frac{\partial f^{(k)}_{n+1}}{\partial\tilde{\sigma}^{(k)}_{n+1}}
\end{aligned} \tag{16}$$

In each of the three equations presented in eq.(16), the k variable represents the iteration step within the iterative process destined to find the solutions of the $\Delta\boldsymbol{\sigma}_{n+1}$, the $\Delta\boldsymbol{\epsilon}^{p}_{n+1}$ and the $\Delta\tilde{\epsilon}_{n+1}$ variables. These solutions are the ones that lead to a simultaneous decrease of the $r_{f,\ n+1}$, $r_{\boldsymbol{\epsilon},\ n+1}$ and $r_{\tilde{\epsilon},\ n+1}$ residues below a predefined tolerance. For the first step of the iterative procedure, $(k=1)$, the residues $r^{(k=1)}_{\boldsymbol{\epsilon},\ n+1}$ and $r^{(k=1)}_{\tilde{\epsilon},\ n+1}$ are null from the abovementioned, and the residue $r^{(k=1)}_{f,\ n+1}$ is obtained by eq.(17):

$$r^{(k=1)}_{f,\ n+1} = f^{(k=1)}_{n+1}\left(\boldsymbol{\sigma}^{trial}_{n+1},\ \tilde{\sigma}_{n}\right) \tag{17}$$

The use of the Newton-Raphson scheme for the solution of the three equations system requires the linearization of the equations. By differentiating, one obtains:

$$\begin{aligned}
r^{(k)}_{f,\ n+1} + \frac{\partial f^{(k)}_{n+1}}{\partial\boldsymbol{\sigma}^{(k)}_{n+1}} d\boldsymbol{\sigma}^{(k+1)}_{n+1} + \frac{\partial f^{(k)}_{n+1}}{\partial\tilde{\sigma}^{(k)}_{n+1}}\ d\tilde{\sigma}^{(k+1)}_{n+1} = 0\\
r^{(k)}_{\boldsymbol{\epsilon},\ n+1} - d\boldsymbol{\epsilon}^{p,\ (k+1)}_{n+1} + d\lambda^{(k+1)}_{n+1}\ \frac{\partial f^{(k)}_{n+1}}{\partial\boldsymbol{\sigma}^{(k)}_{n+1}}\ + \Delta\lambda^{(k)}_{n+1}\left[\frac{\partial^2 f^{(k)}_{n+1}}{\partial\left(\boldsymbol{\sigma}^{(k)}_{n+1}\right)^2} d\boldsymbol{\sigma}^{(k+1)}_{n+1}\ +\right.\\
\left.\frac{\partial^2 f^{(k)}_{n+1}}{\partial\boldsymbol{\sigma}^{(k)}_{n+1}\ \partial\tilde{\sigma}^{(k)}_{n+1}}\ d\tilde{\sigma}^{(k+1)}_{n+1}\right] = 0
\end{aligned} \tag{18}$$

$$r^{(k)}_{\tilde{\epsilon},\ n+1} - d\tilde{\epsilon}^{(k+1)}_{n+1} - d\lambda^{(k+1)}_{n+1}\ \frac{\partial f^{(k)}_{n+1}}{\partial \tilde{\sigma}^{(k)}_{n+1}} - \Delta\lambda^{(k)}_{n+1}\left[\frac{\partial^2 f^{(k)}_{n+1}}{\partial\left(\tilde{\sigma}^{(k)}_{n+1}\right)^2} d\tilde{\sigma}^{(k+1)}_{n+1}\ +\right.$$
$$\left.\frac{\partial^2 f^{(k)}_{n+1}}{\partial \tilde{\sigma}^{(k)}_{n+1}\partial \boldsymbol{\sigma}^{(k)}_{n+1}} d\boldsymbol{\sigma}^{(k+1)}_{n+1}\right] = 0$$

Despite leading to the same result, another common way to present the problem of minimisation of the three residues is by establishing the Jacobian $\boldsymbol{J}$ and solving the following system of linear equations:

$$\boldsymbol{J}^{(k)}_{n+1}\begin{bmatrix} d\boldsymbol{\sigma}^{(k+1)}_{n+1} \\ d\tilde{\epsilon}^{(k+1)}_{n+1} \\ d\lambda^{(k+1)}_{n+1} \end{bmatrix} = \begin{bmatrix} -r^{(k)}_{f,\ n+1} \\ -r^{(k)}_{\boldsymbol{\epsilon},\ n+1} \\ -r^{(k)}_{\tilde{\epsilon},\ n+1} \end{bmatrix} \tag{19}$$

In the present case, the Jacobian may be represented by the following matrix:

$$\boldsymbol{J}^{(k)}_{n+1} = \begin{bmatrix} \dfrac{\partial F_1}{\partial \boldsymbol{\sigma}_{n+1}} & \dfrac{\partial F_1}{\partial \tilde{\epsilon}_{n+1}} & \dfrac{\partial F_1}{\partial \lambda_{n+1}} \\ \dfrac{\partial F_2}{\partial \boldsymbol{\sigma}_{n+1}} & \dfrac{\partial F_2}{\partial \tilde{\epsilon}_{n+1}} & \dfrac{\partial F_2}{\partial \lambda_{n+1}} \\ \dfrac{\partial F_3}{\partial \boldsymbol{\sigma}_{n+1}} & \dfrac{\partial F_3}{\partial \tilde{\epsilon}_{n+1}} & \dfrac{\partial F_3}{\partial \lambda_{n+1}} \end{bmatrix}^{(k)} \tag{20}$$

The functions F_1, F_2 and F_3 are extracted from the equations of the residues $r^{(k)}_{f,\ n+1}$, $r^{(k)}_{\boldsymbol{\epsilon},\ n+1}$ and $r^{(k)}_{\tilde{\epsilon},\ n+1}$ (eqs.(16)). They may be expressed as follows:

$$\begin{aligned} F^{(k)}_1 &= f^{(k)}_{n+1}\left(\boldsymbol{\sigma}^{(k)}_{n+1},\ \tilde{\sigma}^{(k)}_{n+1}\right) \\ F^{(k)}_2 &= \boldsymbol{D}^{-1}\Delta\boldsymbol{\sigma}^{(k)}_{n+1} + \Delta\lambda^{(k)}_{n+1}\ \frac{\partial f^{(k)}_{n+1}}{\partial \boldsymbol{\sigma}^{(k)}_{n+1}} \\ F^{(k)}_3 &= -\Delta\tilde{\epsilon}^{(k)}_{n+1} - \Delta\lambda^{(k)}_{n+1}\ \frac{\partial f^{(k)}_{n+1}}{\partial \tilde{\sigma}^{(k)}_{n+1}} \end{aligned} \tag{21}$$

In eq.(16), the term ' $-\left(\tilde{\epsilon}^{p}_{n+1}\right)^{(k)} + \tilde{\epsilon}^{p}_{n}$ ' was replaced by ' $-\Delta\tilde{\epsilon}^{(k)}_{n+1}$ '. In eq.(16), the term ' $-\left(\boldsymbol{\epsilon}^{p}_{n+1}\right)^{(k)} + \boldsymbol{\epsilon}^{p}_{n}$ ' was replaced by ' $\boldsymbol{D}^{-1}\Delta\boldsymbol{\sigma}^{(k)}_{n+1}$ ', and the equivalence of both terms is further explained. According to the flow rule, the plastic strains vector at the load step '$n+1$' may be defined on the basis of the plastic strain of the former load step, 'n', by the equation:

$$\boldsymbol{\epsilon}^{p}_{n+1} = \boldsymbol{\epsilon}^{p}_{n} + \Delta\boldsymbol{\epsilon}^{p}_{n+1} \ , \tag{22}$$

with the term $\Delta\boldsymbol{\epsilon}^{p}_{n+1}$ being defined by the equation already described in the previous section:

$$\Delta\boldsymbol{\epsilon}^{p}_{n+1} = \Delta\lambda_{n+1} \ \frac{\partial f_{n+1}}{\partial\boldsymbol{\sigma}_{n+1}} \tag{23}$$

Once the plastic strains $\boldsymbol{\epsilon}^{p}_{n+1}$ are known, the final stresses of the corresponding load step may be computed from the equation:

$$\boldsymbol{\sigma}_{n+1} = \boldsymbol{\sigma}^{trial}_{n+1} - \boldsymbol{D}\Delta\boldsymbol{\epsilon}^{p}_{n+1} \ , \tag{24}$$

which may be combined with eq(14) to yield:

$$\boldsymbol{\sigma}_{n+1} - \boldsymbol{\sigma}^{trial}_{n+1} + \Delta\lambda_{n+1} \ \boldsymbol{D} \ \frac{\partial f_{n+1}}{\partial\boldsymbol{\sigma}_{n+1}} = 0 \ , \tag{25}$$

rearranging, and adopting the incremental form, yields:

$$r^{(k)}_{\boldsymbol{\epsilon},\ n+1} = \boldsymbol{D}^{-1}\left(\boldsymbol{\sigma}^{(k)}_{n+1} - \boldsymbol{\sigma}^{trial}_{n+1}\right) + \Delta\lambda^{(k)}_{n+1} \ \frac{\partial f^{(k)}_{n+1}}{\partial\boldsymbol{\sigma}^{(k)}_{n+1}} \tag{26}$$

At last, the final converged values of the unknowns for the step ' $n+1$ ' are obtained trough the successive summation of the increments determined at each iteration from the linear system of eqs.(19), that is:

$$\begin{aligned} \boldsymbol{\sigma}^{(k)}_{n+1} &= \boldsymbol{\sigma}_{n} + \sum_{i=1}^{k} d\boldsymbol{\sigma}^{(i)}_{n+1} \\ \tilde{\epsilon}^{(k)}_{n+1} &= \tilde{\epsilon}_{n} + \sum_{i=1}^{k} d\tilde{\epsilon}^{(i)}_{n+1} \\ \Delta\lambda^{(k)}_{n+1} &= \sum_{i=1}^{k} d\lambda^{(i)}_{n+1} \end{aligned} \tag{27}$$

2.2 First and second order derivatives

The implementation of the equations described above implies some other first order derivatives and the second order derivatives. Those have to be determined, namely:

- the remaining first order derivatives of the functions F_1, F_2 and F_3 with respect to the stress vector $\boldsymbol{\sigma}$, the internal variable or equivalent plastic strain $\tilde{\epsilon}$, and the plastic multiplier λ;
- the fist order derivative of the loading function f with respect to the hardening parameter $\tilde{\sigma}$;
- the second order derivatives of the loading function f, the Ottosen lambda parameter and the stress tensor invariants (I_1, J_2 and J_3) with respect to the stress vector $\boldsymbol{\sigma}$, and the hardening parameter $\tilde{\sigma}$.

These derivatives are quite straightforward but long so, for the sake of clarity of this work, they will not be demonstrated.

3 The Consistent Tangent Elasto-plastic Constitutive Matrix

For the integration of the FEM equilibrium equations within the Newton-Raphson incremental-iterative algorithm framework, it is desirable to obtain and use the consistent tangent constitutive matrix. This procedure contributes to a faster convergence of the algorithm to the equilibrium solution of the combination increment [11]. For this purpose, in the following steps the equation of the tangent constitutive matrix will be derived.
To start with, let one remind the equations in which the derivation of the tangent constitutive matrix will be based. The yield function, as a function of the stress vector and the hardening parameter,

$$f_{n+1} = f_{n+1}(\boldsymbol{\sigma}, \tilde{\sigma}) \ , \tag{28}$$

the constitutive equation, in the incremental form:

$$\Delta\boldsymbol{\sigma}_{n+1} = \boldsymbol{D}\left(\Delta\boldsymbol{\epsilon}_{n+1} - \Delta\boldsymbol{\epsilon}^{p}_{n+1}\right) \ , \tag{29}$$

the flow rule:

$$\Delta\boldsymbol{\epsilon}^{p}_{n+1} = \Delta\lambda_{n+1} \ \frac{\partial f_{n+1}}{\partial\boldsymbol{\sigma}_{n+1}} \ , \tag{30}$$

and the evolution law:

$$\Delta\tilde{\epsilon}_{n+1} = -\Delta\lambda_{n+1}\ \frac{\partial f_{n+1}}{\partial\tilde{\sigma}_{n+1}}\ . \tag{31}$$

The derivation of the consistent tangent matrix for the general return-mapping algorithm requires the determination of the total differentials df_{n+1}, $d\boldsymbol{\sigma}_{n+1}$, $d\boldsymbol{\epsilon}_{n+1}$, and $d\tilde{\epsilon}_{n+1}$. In this fashion, one obtains, for the yield function (known as the normality rule):

$$df_{n+1} = \frac{\partial f_{n+1}}{\partial\boldsymbol{\sigma}_{n+1}}d\boldsymbol{\sigma}_{n+1} + \frac{\partial f_{n+1}}{\partial\tilde{\sigma}_{n+1}}d\tilde{\sigma}_{n+1}\ , \tag{32}$$

for the constitutive equation:

$$d\boldsymbol{\sigma}_{n+1} = \boldsymbol{D}\left(d\boldsymbol{\epsilon}_{n+1} - d\boldsymbol{\epsilon}^{p}_{n+1}\right)\ , \tag{33}$$

for the flow rule:

$$d\boldsymbol{\epsilon}^{p}_{n+1} = d\lambda_{n+1}\ \frac{\partial f_{n+1}}{\partial\boldsymbol{\sigma}_{n+1}} + \Delta\lambda_{n+1}\left(\frac{\partial^2 f_{n+1}}{\partial\boldsymbol{\sigma}^2_{n+1}}d\boldsymbol{\sigma}_{n+1} + \frac{\partial^2 f_{n+1}}{\partial\boldsymbol{\sigma}_{n+1}\partial\tilde{\sigma}_{n+1}}d\tilde{\sigma}_{n+1}\right)\ , \tag{34}$$

and for the evolution law:

$$d\tilde{\epsilon}_{n+1} = -d\lambda_{n+1}\ \frac{\partial f_{n+1}}{\partial\tilde{\sigma}_{n+1}} - \Delta\lambda_{n+1}\left(\frac{\partial^2 f_{n+1}}{\partial\tilde{\sigma}^2_{n+1}}d\tilde{\sigma}_{n+1} + \frac{\partial^2 f_{n+1}}{\partial\tilde{\sigma}_{n+1}\partial\boldsymbol{\sigma}_{n+1}}d\boldsymbol{\sigma}_{n+1}\right)\ . \tag{35}$$

All $n+1$ values correspond to the converged values at the end of the Newton-Raphson iterative procedure, destined to find the equilibrium solution of the load step $n+1$, for each integration point.
Substituting eq.(34) in eq.(33), after some algebraic operations, one obtains:

$$d\boldsymbol{\sigma}_{n+1} = \boldsymbol{H}\left(d\boldsymbol{\epsilon}_{n+1} - d\lambda_{n+1}\ \frac{\partial f_{n+1}}{\partial\boldsymbol{\sigma}_{n+1}} - \Delta\lambda_{n+1}\frac{\partial^2 f_{n+1}}{\partial\boldsymbol{\sigma}_{n+1}\partial\tilde{\sigma}_{n+1}}\ d\tilde{\sigma}_{n+1}\right)\ , \tag{36}$$

where $\boldsymbol{H} = \left(\boldsymbol{D}^{-1} + \Delta\lambda_{n+1}\frac{\partial^2 f_{n+1}}{\partial\boldsymbol{\sigma}^2_{n+1}}\right)^{-1}$ represents the elasto-plastic constitutive tensor.
Substituting the eq.(36) into eq.(32) and acknowledging that while plastic deformation is taking place, for a specific converged solution of a load step, $df_{n+1} = 0$, then one obtains:

$$\begin{aligned}\frac{\partial f_{n+1}}{\partial\boldsymbol{\sigma}_{n+1}}\ \boldsymbol{H}\ d\boldsymbol{\epsilon}_{n+1}\ &= d\lambda_{n+1}\ \frac{\partial f_{n+1}}{\partial\boldsymbol{\sigma}_{n+1}}\ \boldsymbol{H}\ \frac{\partial f_{n+1}}{\partial\boldsymbol{\sigma}_{n+1}}\ + \\ &+\ \left(\Delta\lambda_{n+1}\ \frac{\partial f_{n+1}}{\partial\boldsymbol{\sigma}_{n+1}}\ \boldsymbol{H}\ \frac{\partial^2 f_{n+1}}{\partial\boldsymbol{\sigma}_{n+1}\partial\tilde{\sigma}_{n+1}}\ -\ \frac{\partial f_{n+1}}{\partial\tilde{\sigma}_{n+1}}\right)\ d\tilde{\sigma}_{n+1}\ .\end{aligned} \tag{37}$$

Substituting eq.(36) into eq.(35), and making use of $d\tilde{\sigma} = h\ d\tilde{\epsilon}$, after some simplifications one obtains:

$$\left(-\frac{\partial f_{n+1}}{\partial \tilde{\sigma}_{n+1}} + \Delta\lambda_{n+1}\ \frac{\partial^2 f_{n+1}}{\partial \tilde{\sigma}_{n+1}\partial \boldsymbol{\sigma}_{n+1}}\boldsymbol{H}\frac{\partial f_{n+1}}{\partial \boldsymbol{\sigma}_{n+1}}\right)\ d\lambda_{n+1} + \left(-h\ \Delta\lambda_{n+1}\ \frac{\partial^2 f_{n+1}}{\partial \tilde{\sigma}_{n+1}^2} + h\ \Delta\lambda_{n+1}^2\ \frac{\partial^2 f_{n+1}}{\partial \tilde{\sigma}_{n+1}\partial \boldsymbol{\sigma}_{n+1}}\boldsymbol{H}\frac{\partial^2 f_{n+1}}{\partial \boldsymbol{\sigma}_{n+1}\partial \tilde{\sigma}_{n+1}} - 1\right)\ d\tilde{\epsilon}_{n+1} = \Delta\lambda_{n+1}\ \frac{\partial^2 f_{n+1}}{\partial \tilde{\sigma}_{n+1}\partial \boldsymbol{\sigma}_{n+1}}\boldsymbol{H} d\boldsymbol{\epsilon}_{n+1}\ . \tag{38}$$

In order to be possible the substitution of eq.(37) and eq.(38) into eq.(36), the first and the second must be described explicitly with respect to $(d\lambda_{n+1})$ and $(\Delta\lambda_{n+1}\ \tilde{\epsilon}_{n+1})$. In this fashion, one obtains, for eq.(37):

$$\left(\frac{\partial f_{n+1}}{\partial \boldsymbol{\sigma}_{n+1}}\ \boldsymbol{H}\ \frac{\partial f_{n+1}}{\partial \boldsymbol{\sigma}_{n+1}}\right)\ d\lambda_{n+1} + \left(h\ \frac{\partial f_{n+1}}{\partial \boldsymbol{\sigma}_{n+1}}\ \boldsymbol{H}\ \frac{\partial^2 f_{n+1}}{\partial \boldsymbol{\sigma}_{n+1}\partial \tilde{\sigma}_{n+1}} - \frac{h}{\Delta\lambda_{n+1}}\frac{\partial f_{n+1}}{\partial \tilde{\sigma}_{n+1}}\right)\ \Delta\lambda_{n+1}\ d\tilde{\epsilon}_{n+1} = \frac{\partial f_{n+1}}{\partial \boldsymbol{\sigma}_{n+1}}\ \boldsymbol{H}\ d\boldsymbol{\epsilon}_{n+1}\ , \tag{39}$$

and for eq.(38):

$$\left(-\frac{h}{\Delta\lambda_{n+1}}\frac{\partial f_{n+1}}{\partial \tilde{\sigma}_{n+1}} + h\ \frac{\partial^2 f_{n+1}}{\partial \tilde{\sigma}_{n+1}\partial \boldsymbol{\sigma}_{n+1}}\boldsymbol{H}\frac{\partial f_{n+1}}{\partial \boldsymbol{\sigma}_{n+1}}\right) d\lambda_{n+1} + \left(\frac{-h^2}{\Delta\lambda_{n+1}}\frac{\partial^2 f_{n+1}}{\partial \tilde{\sigma}_{n+1}^2} + h^2\ \frac{\partial^2 f_{n+1}}{\partial \tilde{\sigma}_{n+1}\partial \boldsymbol{\sigma}_{n+1}}\boldsymbol{H}\frac{\partial^2 f_{n+1}}{\partial \boldsymbol{\sigma}_{n+1}\partial \tilde{\sigma}_{n+1}} - \frac{h}{\Delta\lambda_{n+1}^2}\right)\ \Delta\lambda_{n+1}\ d\tilde{\epsilon}_{n+1} = h\ \frac{\partial^2 f_{n+1}}{\partial \tilde{\sigma}_{n+1}\partial \boldsymbol{\sigma}_{n+1}}\boldsymbol{H} d\boldsymbol{\epsilon}_{n+1}\ . \tag{40}$$

The values of $(d\lambda_{n+1})$ and $(\Delta\lambda_{n+1}\ d\tilde{\epsilon}_{n+1})$ may be obtained by solving the system of the two eqs.(39) and (41), by the following:

$$\begin{bmatrix} d\lambda_{n+1} \\ \Delta\lambda_{n+1}\ d\tilde{\epsilon}_{n+1} \end{bmatrix} = \begin{bmatrix} A_{11} & A_{12} \\ A_{21} & A_{22} \end{bmatrix}^{-1} \begin{bmatrix} B_1 \\ B_2 \end{bmatrix} \tag{41}$$

with:

$$A_{11} = \frac{\partial f_{n+1}}{\partial \boldsymbol{\sigma}_{n+1}}\ \boldsymbol{H}\frac{\partial f_{n+1}}{\partial \boldsymbol{\sigma}_{n+1}}\ ,$$

$$
\begin{aligned}
A_{12} &= h\ \frac{\partial f_{n+1}}{\partial \boldsymbol{\sigma}_{n+1}} \boldsymbol{H} \frac{\partial^2 f_{n+1}}{\partial \boldsymbol{\sigma}_{n+1} \partial \tilde{\sigma}_{n+1}} \ - \ \frac{h}{\Delta\lambda_{n+1}} \frac{\partial f_{n+1}}{\partial \tilde{\sigma}_{n+1}} \ , \\
A_{21} &= -\frac{h}{\Delta\lambda_{n+1}} \frac{\partial f_{n+1}}{\partial \tilde{\sigma}_{n+1}} \ + \ h\ \frac{\partial^2 f_{n+1}}{\partial \tilde{\sigma}_{n+1} \partial \boldsymbol{\sigma}_{n+1}} \boldsymbol{H} \frac{\partial f_{n+1}}{\partial \boldsymbol{\sigma}_{n+1}} \ , \\
A_{22} &= \frac{-h^2}{\Delta\lambda_{n+1}} \frac{\partial^2 f_{n+1}}{\partial \tilde{\sigma}_{n+1}^2} \ + h^2\ \frac{\partial^2 f_{n+1}}{\partial \tilde{\sigma}_{n+1} \partial \boldsymbol{\sigma}_{n+1}} \boldsymbol{H} \frac{\partial^2 f_{n+1}}{\partial \boldsymbol{\sigma}_{n+1} \partial \tilde{\sigma}_{n+1}} - \frac{h}{\Delta\lambda_{n+1}^2} \ , \\
B_1 &= \ \frac{\partial f_{n+1}}{\partial \boldsymbol{\sigma}_{n+1}} \boldsymbol{H} d\boldsymbol{\epsilon}_{n+1} \ , \\
B_2 &= \ h\ \frac{\partial^2 f_{n+1}}{\partial \tilde{\sigma}_{n+1} \partial \boldsymbol{\sigma}_{n+1}} \boldsymbol{H} d\boldsymbol{\epsilon}_{n+1} \ .
\end{aligned}
\tag{42}
$$

If it is assumed that:

$$
\begin{bmatrix} A_{11} & A_{12} \\ A_{21} & A_{22} \end{bmatrix}^{-1} = \begin{bmatrix} a_{11} & a_{12} \\ a_{21} & a_{22} \end{bmatrix} \ , \tag{43}
$$

then, making use of the matrix inversion algebra to compute the inverse of a second rank matrix, one obtains:

$$
\begin{aligned}
a_{11} &= \frac{A_{22}}{A_{11}\ A_{22} - A_{12}\ A_{21}} \ , \\
a_{12} = a_{21} &= -\frac{A_{12}}{A_{11}\ A_{22} - A_{12}\ A_{21}} \ , \\
a_{22} &= \frac{A_{11}}{A_{11}\ A_{22} - A_{12}\ A_{21}} \ .
\end{aligned}
\tag{44}
$$

One may also rewrite:

$$
\begin{bmatrix} B_1 \\ B_2 \end{bmatrix} = \begin{bmatrix} \boldsymbol{b}_1 \\ \boldsymbol{b}_2 \end{bmatrix} \ d\boldsymbol{\epsilon}_{n+1} \ , \tag{45}
$$

and then, based on eqs.(41) and (45), one may rewrite the eq.(36) in the following fashion:

$$
\begin{aligned}
d\boldsymbol{\sigma}_{n+1} = \boldsymbol{H} \Bigg(\boldsymbol{I} - \frac{\partial f_{n+1}}{\partial \boldsymbol{\sigma}_{n+1}} \left(a_{11}\ \boldsymbol{b}_1 + a_{12}\ \boldsymbol{b}_2\right) - \\
- \ h\ \frac{\partial^2 f_{n+1}}{\partial \boldsymbol{\sigma}_{n+1} \partial \tilde{\sigma}_{n+1}} \left(a_{21}\ \boldsymbol{b}_1 + a_{22}\ \boldsymbol{b}_2\right) \Bigg) \ d\boldsymbol{\epsilon}_{n+1} \ ,
\end{aligned}
\tag{46}
$$

or rearranging:

$$d\boldsymbol{\sigma}_{n+1} = \Bigg(\boldsymbol{H} \; - \; a_{11} \; \boldsymbol{H} \frac{\partial f_{n+1}}{\partial \boldsymbol{\sigma}_{n+1}} \frac{\partial f_{n+1}}{\partial \boldsymbol{\sigma}_{n+1}} \boldsymbol{H} \; - \; h \; a_{12} \; \boldsymbol{H} \frac{\partial f_{n+1}}{\partial \boldsymbol{\sigma}_{n+1}} \frac{\partial^2 f_{n+1}}{\partial \tilde{\sigma}_{n+1} \partial \boldsymbol{\sigma}_{n+1}} \boldsymbol{H} \; -$$
$$- \; h \; a_{21} \; \boldsymbol{H} \frac{\partial^2 f_{n+1}}{\partial \boldsymbol{\sigma}_{n+1} \tilde{\sigma}_{n+1}} \frac{\partial f_{n+1}}{\partial \boldsymbol{\sigma}_{n+1}} \boldsymbol{H} \; - \; h^2 \; a_{22} \; \boldsymbol{H} \frac{\partial^2 f_{n+1}}{\partial \boldsymbol{\sigma}_{n+1} \partial \tilde{\sigma}_{n+1}} \frac{\partial^2 f_{n+1}}{\partial \tilde{\sigma}_{n+1} \partial \boldsymbol{\sigma}_{n+1}} \boldsymbol{H} \Bigg) d\boldsymbol{\epsilon}_{n+1} \tag{47}$$

or, in a condensed expression:

$$d\boldsymbol{\sigma}_{n+1} = \left(\boldsymbol{H} - \sum_{i=1}^{2} \sum_{i=1}^{2} a_{ij} \; \boldsymbol{c}_i \boldsymbol{c}_j \right) d\boldsymbol{\epsilon}_{n+1} \tag{48}$$

with:

$$\boldsymbol{c}_1 = \boldsymbol{H} \frac{\partial f_{n+1}}{\partial \boldsymbol{\sigma}_{n+1}} \quad ; \quad \boldsymbol{c}_2 = \; h \; \boldsymbol{H} \frac{\partial^2 f_{n+1}}{\partial \tilde{\sigma}_{n+1} \partial \boldsymbol{\sigma}_{n+1}} \; . \tag{49}$$

So finally one may state that the expression of the consistent tangent constitutive matrix is the following:

$$\boldsymbol{D}_{ep} = \boldsymbol{H} - \sum_{i=1}^{2} \sum_{i=1}^{2} a_{ij} \; \boldsymbol{c}_i \boldsymbol{c}_j \; , \tag{50}$$

and coincides with the elastic constitutive matrix when the behaviour remains elastic, as it can be demonstrated by replacing in the previous equations the $\Delta\lambda_{n+1}$ parameter by 0. Despite formally appealing and theoretically much more efficient (quadratic convergence within the Newton-Raphson incremental-iterative procedure), the derived consistent tangent elastoplastic matrix is considerably more difficult to determine and numerically more demanding, with increased risk of instability mainly associated with the loss of non-singularity. Alternativelly, in the cases where a simpler porcedure is preferred, a simpler and more common form of the consistent tangent constitutive matrix may be determined. With this procedue, however, quadratic convergence is not assured. In the present case, if one neglects the hardening parameter dependency of the first term of eq.(2) ,

$$f(\boldsymbol{\sigma}, \tilde{\sigma}) = \left[\alpha J_2 + f_{cm} \left(\lambda \sqrt{J_2} + \beta I_1 \right) \right]^{\frac{1}{2}} - \tilde{\sigma} \tag{51}$$

that is to say $\frac{\partial f_{n+1}}{\partial \tilde{\sigma}_{n+1}} = -1$, one obtains, for the normality rule:

$$df_{n+1} = \frac{\partial f_{n+1}}{\partial \boldsymbol{\sigma}_{n+1}} d\boldsymbol{\sigma}_{n+1} - h d\tilde{\epsilon} \; , \tag{52}$$

and for the flow rule and the evolution law:

$$d\boldsymbol{\epsilon}^p_{n+1} = d\lambda_{n+1}\,\frac{\partial f_{n+1}}{\partial \boldsymbol{\sigma}_{n+1}} + \Delta\lambda_{n+1}\frac{\partial^2 f_{n+1}}{\partial \boldsymbol{\sigma}^2_{n+1}},$$
$$d\tilde{\epsilon}_{n+1} = d\lambda_{n+1}. \tag{53}$$

allowing us to rewrite the eq.(36), after substitution of eq.(53) into eq.(33), in the following fashion:

$$d\boldsymbol{\sigma}_{n+1} = \boldsymbol{H}\ \left(d\boldsymbol{\epsilon}_{n+1} - d\lambda_{n+1}\,\frac{\partial f_{n+1}}{\partial \boldsymbol{\sigma}_{n+1}}\right)\ , \tag{54}$$

Following the same procedure as before for the derivation of $\boldsymbol{D}_{ep}$, we first derive the expression of the plastic multiplier differential, $d\lambda_{n+1}$:

$$d\lambda_{n+1} = d\tilde{\epsilon}_{n+1} = \frac{\dfrac{\partial f_{n+1}}{\partial \boldsymbol{\sigma}_{n+1}}\boldsymbol{H}\,d\boldsymbol{\epsilon}_{n+1}}{h + \dfrac{\partial f_{n+1}}{\partial \boldsymbol{\sigma}_{n+1}}\boldsymbol{H}\dfrac{\partial f_{n+1}}{\partial \boldsymbol{\sigma}_{n+1}}}\ , \tag{55}$$

and then, again by substitution into eq.(54), one obtains:

$$d\boldsymbol{\sigma}_{n+1} = \left(\boldsymbol{H} - \frac{\boldsymbol{H}\dfrac{\partial f_{n+1}}{\partial \boldsymbol{\sigma}_{n+1}}\dfrac{\partial f_{n+1}}{\partial \boldsymbol{\sigma}_{n+1}}\boldsymbol{H}}{h + \dfrac{\partial f_{n+1}}{\partial \boldsymbol{\sigma}_{n+1}}\boldsymbol{H}\dfrac{\partial f_{n+1}}{\partial \boldsymbol{\sigma}_{n+1}}}\right) d\boldsymbol{\epsilon}_{n+1} \tag{56}$$

conforming a more frequent form of the elasto-plastic tangent constitutive matrix. Obviously, this procedure does not guarantees quadratic convergence for the iterative procedure.

4 RESULTS AND DISCUSSION

The elastoplastic model described above was implemented in a Finite Element Method based software called FEMIX [12]. In order to assess the model behaviour in different stress combinations, in the following studies the 8-node cubic element with one integration point was used. The elastic stage of the material behaviour was reduced to only 10% of the ultimate strength in uniaxial compression ($0.1 f_{cm}$).

For the simulation of the uniaxial compression test, the loading setup consisted on a constant prescribed displacement in the direction of $x3$. Both cube faces perpendicular to $x1$ and $x2$ were free. In the case of the biaxial test, similar displacement increments were prescribed in $x3$ and $x2$, keeping the cube faces perpendicular to $x1$ free to deform.

In figure 3 the deviatoric plane of the loading surface is depicted for two distinct levels of hydrostatic pressure. The type of concrete considered has a compressive strength of 40 MPa. In the first diagram, (a), the deviatoric plane of the loading surfaces corresponding to the hardening parameter assuming the values of 10, 20, 30 and 40 MPa is depicted. In this first situation, the deviatoric plane is determined for a hydrostatic pressure of 10% of the compressive strength, what may be considered as a low value of the normalized hydrostatic pressure. In the second diagram, (b), the deviatoric plane is again depicted for the same 10, 20, 30 and 40 MPa of hardening parameter loading surfaces, but this time for a hydrostatic pressure of 10 times more than the compressive strength, what may be considered as a high value of the normalized hydrostatic pressure.

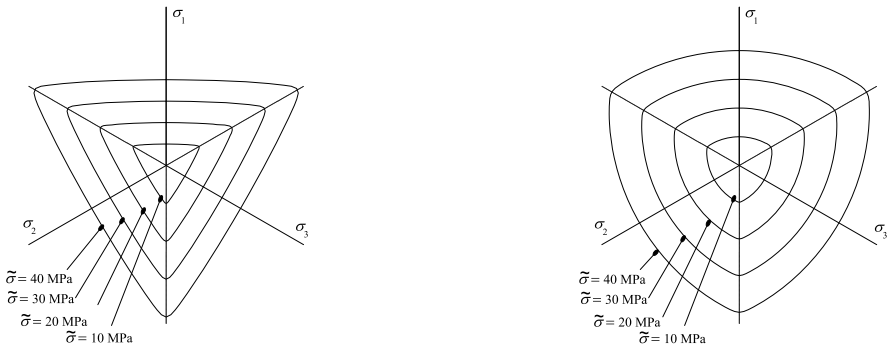

(a) (b)

Figure 3: Representation of the loading function in the Haigh-Westergaard stress space, for concrete of $f_c = 40$ MPa. Deviatoric planes for hardening parameter values of 10, 20, 30 and 40 MPa: (a) for low hydrostatic stress ($I_1/f_c = 0.1$) and (b) high hydrostatic stress ($I_1/f_c = 10.0$).

When considering the equation of the loading surface (eq.(2)), it could be not immediately inferable that the loading surfaces corresponding to different values of the hardening parameter are self-similar with respect to the origin, despite we are dealing only with one hardening parameter and with isotropic hardening. In eq.(2) the efect of the hardening parameter on the expansion or contraction of the loading surface is not explicitelly defined. In fact, the equation of this loading surface does not follow the more common form of the general equation of isotropic loading surfaces, where the hardening parameter effect on the expansion or contraction of the loading surface is explicit [7]:

$$f(\boldsymbol{\sigma}, \tilde{\sigma}) = F(\boldsymbol{\sigma}) - \tilde{\sigma} \tag{57}$$

It may be observed from figures 3, however, that the different loading surfaces are self-similar with respect to the origin, as demonstrated by the visibly parallel curves obtained for both low and high hydrostatic pressure levels.

In figure 4(a) is depicted the axial stress *vs* axial strain results obtained for the uniaxial and biaxial tests. The uniaxial curve is coincident with the curve of uniaxial stress-strain behaviour of a concrete cylinder, obtained from [1] and used in the model to define the evolution of the hardening parameter. In this case, a concrete compressive strength of 40 MPa was considered, so the model was able to follow quite smoothly the hardening/softening behaviour of the concrete cube under uniaxial compression. This mainly agrees with the results obtained by several researchers (see for example [4], [13], [5], [6],) in the characterization of uniaxial compression behaviour of concrete, if the usual post-peak results scatter are disregarded due to the well-known material and specimen size scale effects and different testing boundary conditions.

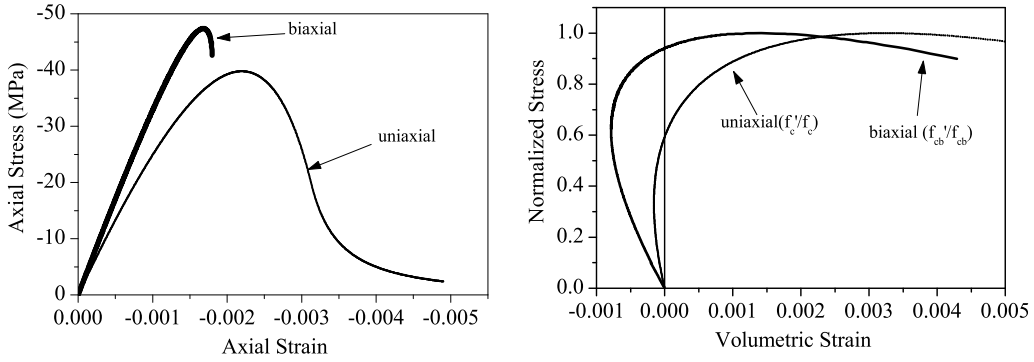

Figure 4: Model results obtained for (a) stress *vs* strain and (b) volumetric strain *vs* normalized stress.

In the case of the biaxial compression, the results obtained are somewhat more brittle than expected, at least while comparing them with the available experimental results of other researchers. The relation between the peak stress in biaxial and uniaxial compression is close, however, to the values obtained experimentally. In the present case, the value obtained was of 1.185. Actually, this value may change with the concrete strength, as suggested by [6]. Observing the results of figure 4(b), in a general perspective the experimentally observed behaviour of the material in terms of volume change is well captured, with an initial decrease in volumetric strain, followed by a gradual increase that becomes more intense for high load values and during de softening branch of the loading curves. These volumetric changes and change transitions are much more pronounced for the biaxial test-setup, as expected and in agreement with the experimentally observed ([4]). It seems, however, that the obtained values are somewhat underestimated, since experimental results point for a greater decrease of volumetric strain in the hardening branch of the loading curve. Eventually, this difference could be attenuated by tuning the value adopted for the Poisson's ratio, rarely discussed and presented in the bibliography.

5 CONCLUSIONS

The utility and viability of the application of the Ottossen failure criterion as a loading surface for the modelling of the nonlinear behaviour of concrete under multiaxial states of stress was briefly assessed. An increased difficulty emerged while generalizing the Ottosen failure criterion in a hardening/softening framework, since the expression of the loading surface does not fit the general and simpler form of the isotropic models, where the hardening parameter is explicitly defined. It was possible to confirm, however, that the loading surfaces remain self-similar with respect to the origin.

The implementation of an isotropic hardening algorithm restricts our study and the model applicability almost to the cases where monotonic static loading occurs. The limitations of isotropic models to simulate cyclic or reversed loadings are well known. However, the characterization of the model parameters based on experimental results is much simpler and easier. In the cases of cyclic or reversed loading, some particular measures are needed to reformulate the numerical implementation.

In a general view, the model was able to capture the main features of uniaxial and biaxial behaviour. The obtained stress-strain relations agree quite well with the available experimental results obtained by other researchers, and the model smoothly follows the expected behaviour. The biaxial results in terms of stress-strain relation show, however, a behaviour relatively more brittle than expected, when comparing it with the experimental results obtained by other researchers. In terms of volumetric changes, the overall behaviour obtained follows the expected, with the initial decrease in volume followed by a growing increase in the last stages of the hardening branch and during softening. The results seem, though, somewhat overestimated in terms of volume decrease, mainly in the pre-peak regions.

6 ACKNOWLEDGMENTS

The first author would also like thank the generous help and wise thoughts of Prof. Leif Otto Nielsen, from DTU. Special thanks also to the Portuguese National Science Foundation for the financial support, through grant SFRH / BD / 36515 / 2007, supported by POPH - QREN, the Social European Fund and the MCTES.

REFERENCES

[1] CEB-FIB, *CEB-FIP Model Code 1990 - Design Code*, Thomas Telford, (1993).

[2] W.F. Chen, *Plasticity in reinforced concrete*, McGraw Hill, (1982).

[3] N.S. Ottosen, *Nonlinear Finite Element analysis of concrete structures*, technical report, Riso Natinal Labortory - Denmark, (1980).

[4] H. Kupfer, H.K. Hilsdorf and H.Rusch. Behaviour of concrete under biaxial stresses, *ACI Journal*, Vol.66, pp.656–666, (1969).

[5] P. Grassl, K. Lundgren, K. Gylltoft. Concrete in compression: a plasticity theory with a novel hardening law, *Int Journ. of Sol. and Str.*, Vol. 39, pp.5205–5223, (2002).

[6] V.K. Papanikolaou, A.J. Kappos. Confinement-sensitive plasticity model for concrete in triaxial compression, *Int Journ. of Sol. and Str.*, Vol. 44, pp.7021–7048, (2007).

[7] F.K.G. Odqvist. Die verfestigung von flusseisenahnlichen korpen, *Ein beitrag zur plastizitiitstheorie* Zeit. Angew. Math. Und Mech., Vol. 13, pp. 360-363,(1933).

[8] G. Hofstetter and H.A. Mang, *Computational mechanics of reinforced concrete structures*, Friedr. Vieweg & Sohn Verlagsgesellschaft mbH, (1995).

[9] O.C. Zienkiewicz and R.L. Taylor, *The finite element method*, McGraw Hill, Vol. I., (1989), Vol. II., (1991).

[10] M. Ristinmaa, M. Wallin and N.S. Ottosen. Termodynamic format and heat generation of isotropic hardening plasticity, *Acta Mechanica*, April 2007 (published online).

[11] J.C. Simo and T.J. Hughes, *Elastoplasticity and viscoplasticity - computatinal aspects*, Springer, (1988).

[12] J.M. Sena-Cruz, J.A.O. Barros, A.F.M. Azevedo, A.V. Ventura Gouveia. Numerical simulation of the nonlinear behavior of RC beams strengthened with NSM CFRP strips, *CMNE 2007 - Congress on Numerical Methods in Engineering and XXVIII CILAMCE - Iberian Latin American Congress on Computational Methods in Engineering*, Abstract pp. 289, Paper nº 485 (published in CD) - FEUP, 20 pp., (2007).

[13] J. van Mier, *Fracture processes of concrete*, CRC Press, (1997).